RSC Advances

ROYAL SOCIETY OF CHEMISTRY

www.rsc.org/advances

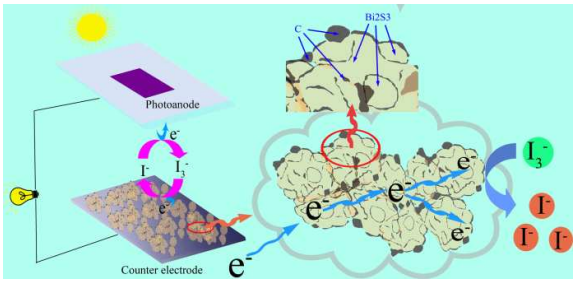

The synergistic effect of the combination of conductive carbon and Bi_2S_3 can significantly improve the photovoltaic performance of the DSSCs.

Cite this: DOI: 10.1039/c0xx00000x

www.rsc.org/xxxxxx

ARTICLE TYPE

Facile synthesis of Bi_2S_3-C composite microspheres as low-cost counter electrodes for dye-sensitized solar cells

Xue-Qin Zuo[a], Xiao Yang [a], Lei Zhou[a], Bo Yang[a], Guang Li*[ab], Huai-Bao Tang [a], Hai-Jun Zhang [a], Ming-Zai Wu [ab], Yong-Qing Ma [ab] and Shao-Wei Jin [ab]

Received (in XXX, XXX) Xth XXXXXXXXX 20XX, Accepted Xth XXXXXXXXX 20XX
DOI: 10.1039/b000000x

Porous bismuth sulfide-carbon (Bi_2S_3-C) composite microspheres were synthesized via a facile solvothermal route and served as a low-cost counter electrode material for Pt-free dye-sensitized solar cells (DSSCs). The electrochemical performance analysis indicates that the Bi_2S_3-C electrode has lower charge transfer resistance on the electrolyte/electrode interface, smaller Nernst diffusion impedance of iodide in electrolyte and higher catalytic ability than bare Bi_2S_3 electrode. After optimization the content of carbon, the DSSC with the Bi_2S_3-C counter electrode exhibit an excellent power conversion efficiency of 6.72%, which is comparable to that of the Pt-based DSSC (6.74%).

Introduction

In the past decade, dye-sensitized solar cells (DSSCs) have attracted extensive attention due to their easy fabrication, low-cost and environment friendliness.[1,2] Generally, a typical DSSC is composed of a dye sensitized photoanode,[3-6] a liquid electrolyte with iodide/triiodide (I^-/I_3^-) redox couples and a catalytic counter electrode (CE). As an indispensable component of DSSCs, CEs collect electrons from external circuit and promote the reduction of triiodide. The conventional CEs are magnetron sputtering deposited or thermally decomposed Pt on rigid fluorine-doped tin oxide (FTO) substrates, which have shown remarkable electrocatalytic activity for the regeneration of iodide from triiodide. However, the high price of metal Pt restrains the large-scale manufacturing of DSSCs. Therefore, it is necessary to explore low cost and effective non-Pt CEs. Fortunately, many economic materials have shown excellent catalytic performance as Pt CEs, such as carbonaceous materials,[7-9] conducting polymers[10-12] and metal nitrides, oxides and sulfides.[13-21] Among them, metal sulfides gained more attention due to their facile preparation conditions and relatively low toxicity.

As a well-known layered semiconductor, bismuth sulfide (Bi_2S_3) has many widely applications in electronic and optoelectronic devices,[22] hydrogen storage materials[23,24] and lithium ion batteries.[25,26] Particularly, Bi_2S_3 is considered as a potential material for photoelectrochemical solar cells by virtue of its small band gap, high absorption coefficient and reasonable energy conversion efficiency.[27] However, to our knowledge, few researches have reported on the application of Bi_2S_3 as CEs in DSSCs except for the works by Liu's group[28,29] and Li's group.[30] In 2012, Liu et al. compared the catalytic activities of different facets within Bi_2S_3 through density functional theory computations. Then, they successfully synthesized flower-like Bi_2S_3 nanostructures with predominantly exposed (130) and (211) facets and obtained photovoltaic efficiencies of 3.5% and 1.9% within these differently faceted Bi_2S_3 based DSSCs, respectively. Subsequently Li et al. prepared Bi_2S_3 microspheres grown on the graphene by two-step solvothermal method and used as CE for the DSSC system. The power conversion efficiency of Bi_2S_3/graphene hybrid material boosted to 5.5%. This remarkable improvement of the conversion efficiency is mainly due to the efficient electron transport network provided by graphene. In fact, many efforts have recently been devoted to investigate the synergistic effect in the combination of nanomaterials and carbon materials. For example, Ma's group reported two composites of MoC and WC embedded in ordered carbon materials and employed them as the CE materials for DSSCs. The results indicated that both of them have superior catalytic performance to the expensive Pt CE.[31] Li et al. also presented an improved photovoltaic efficiency of DSSC with TiN nanoparticles and carbon black composite as CE.[32] And then, Yue et al. utilized high porous MoS_2-C hybrid film as the pt-free CE materials for DSSC and achieved a high photovoltaic efficiency of 7.69 %.[18] Besides, Wang et al. synthesized a carbon-coated WS_2 material using a simple method. The DSSC assembled with this carbide-based CE also showed fantastic photovoltaic performance.[33]

Herein, a composite material of Bi_2S_3 and conductive carbon was prepared by a one-step solvothermal route, and investigated

[a] *School of Physics and Materials Science, Anhui University, Hefei 230601, China*
[b] *Anhui Key Laboratory of Information Materials and Devices, Hefei 230601, China. Fax: +86 0551 63861992; Tel.: +86 0551 63861867; E-mail: liguang1971@ahu.edu.cn (G. Li)*

as CEs for Pt-free DSSCs. As far as we know, this is the first report on the utilization of Bi_2S_3-C composite material as CEs for DSSCs. Based on the beneficial synergetic effect of Bi_2S_3 and carbon, the DSSC assembled with this composite material CE exhibits excellent electrocatalytic activity and achieves a high photovoltaic conventional efficiency of 6.72%. Compared with Li et al. study, our present work has several advantages, namely 1) replace graphene with carbon to improve the conductivity in preparation process, which means the complex preparation process of graphene is avoidable; 2) use a facile one-step solvothermal approach instead of two-step solvothermal approach; and 3) derive more excellent catalytic material than Bi_2S_3/graphene composite.

Experimental

Synthesis of Bi_2S_3 and Bi_2S_3-C composite materials

The Bi_2S_3-C composite materials were prepared by using analytical-grade bismuth nitrate ($Bi(NO_3)_3{\cdot}5H_2O$) and L-cysteine ($C_3H_7NO_2S$), without further purification. The typical synthesis procedure as follows: 2 mM $Bi(NO_3)_3{\cdot}5H_2O$ and 6 mM L-cysteine were dissolved in 30 mL anhydrous ethanol and continuously stirred for 2 h to form a homogeneous solution. Afterward, 5 mg, 10 mg, 20 mg and 30 mg glucose powder were added into the solution, followed by further stirred for another 30 min. The solution was transferred to a 50 mL Teflon-lined stainless steel autoclave, maintained at 150 °C for 24 h, and then cooled to room temperature naturally. The black precipitate was collected by centrifugation, washed several times using deionized water and anhydrous ethanol to remove the possible remaining cations and anions, and then dried in an oven at 60 °C for 8 h for further characterization purposes. The final samples were denoted to Bi_2S_3-0.39-C, Bi_2S_3-0.77-C, Bi_2S_3-1.53-C and Bi_2S_3-2.28-C, respectively. The values 0.39, 0.77, 1.53, and 2.28 represent the contents of carbon are 0.39 wt.%, 0.77 wt.%, 1.53 wt.%, and 2.28 wt.% in the composite materials, respectively.

Pure Bi_2S_3 were synthesized according to the same method of preparing Bi_2S_3-C composites, but only replaced glucose with 0.3 g surfactant PVP 40000.

Fabrication of counter electrodes

To prepare CEs, 0.1 g Bi_2S_3 and Bi_2S_3-C powders were respectively mixed with 0.025 g Polyethylene glycol, and then dispersed into 4 ml anhydrous ethanol followed by stirring to form a fluid mixture. Afterward, a film was made using the doctor-blade technique on FTO conductive glass. The films were annealed at 430 ℃ for 1 h at the protection of argon atmosphere, and then the CEs were obtained. As a comparison, Pt CEs were purchased from Wuhan Georgi science instrument Co. Ltd (Wuhan, Hubei, China).

Assembly of DSSCs

Firstly, the TiO_2 photoanodes were soaked overnight in the N-719 dye solution (0.3mM in the solvent of ethanol). TiO_2 photoanodes were obtained from Dalian HeptaChroma Solar Technology Development Co. Ltd (Dalian, Liaoning, China). Then, the dye-sensitized TiO_2 photoanodes were washed with anhydrous ethanol and dried in the hot air. Finally, the TiO_2 photoanodes were fabricated with the prepared CEs with the injection of redox shuttle electrolyte (0.5M LiI, 0.05M I_2, 0.6M 1-propy1-2, 3-dimethylimidazolium iodide and 0.5M 4-tert-buylpyridine with acetonitrile as the solvent). The effective areas of all cells are 0.5 ×0.5 cm^2.

Characterizations and measurements

The compositions of the as-synthesized samples were characterized by X-ray diffraction (XRD) under a Rigaku D/Max-2500 X-ray diffractometer with Cu Kα radiation (λ= 0.154056 nm). The Raman spectra were recorded with a laser confocal micro Raman spectrometer (Invia-Reflex, Renishaw, UK) at 532 nm with a 100X objective. The sizes and morphologies of Bi_2S_3 and Bi_2S_3-C samples were investigated by scanning electron microscopy (SEM; S-4800, Hitachi, Japan) equipped with energy dispersive spectroscopy (EDS) and transmission electron microscopy (TEM; JEM-2100, JEOL, Japan). Nitrogen adsorption and desoroption isotherms were measured on a Tristar II 3020 automated surface area and pore analyzer. The catalytic activity of the various CEs were characterized by Cyclic voltammetry (CV) tests, which were implemented on an electrochemical workstation (ZAHNER ZENNIUM CIMPS-1, Germany) equipped with a three-electrode system in an anhydrous acetonitrile solution consisting of 0.1 M $LiClO_4$, 10 mM LiI, and 1 mM I_2 at a scan rate of 50 $mV{\cdot}S^{-1}$. The Electrochemical impedance spectroscopy (EIS) and Tafal polarization measurements were executed on symmetric cells containing two identical electrodes, using an impedance measurement unit of workstation in the frequency range 0.1-10^6 Hz with an ac amplitude of 10 mV. The photocurrent density-voltage (*J -V*) curves were measured using a Keithley 2410 digital source meter under the illumination of AM 1.5G simulate solar light (100 $mW{\cdot}cm^{-2}$), which was calibrated by a Si reference cell beforehand. All the measurements were performed at ambient temperature.

Results and discussion

Characterization of the as-synthesized materials

Fig.1 shows the XRD diffraction patterns of Bi_2S_3 and Bi_2S_3-C nanomaterials synthesized by facile solvothermal process. All of the diffraction peaks in both patterns can be readily assigned to the orthorhombic phase Bi_2S_3 (PDF# 17-0320). The derived lattice constants are a = 1.1149 nm, b = 1.1126 nm, and c = 0.3985 nm, which are in good coincidence with the reported values for Bi_2S_3 (a = 1.1149 nm, b = 1.1304 nm, and c = 0.3981 nm).[24,25] Comparing the XRD patterns of Bi_2S_3 and Bi_2S_3-C materials in detail, we found non-existence of the carbon-related characterized peaks in Bi_2S_3-C XRD pattern, denoting the amorphous carbon derived from glucose.[34]

To further confirm the microstructure of carbon, Raman spectroscopy was executed on the pristine Bi_2S_3 and Bi_2S_3-C composite materials. As shown in Fig. 2, both of the samples present scattering bands at 138, 259, 348, 510, 651 and 956 cm^{-1}. Except for the peak at 138 cm^{-1}, all other peaks are well consistent with the reported results of Bi_2S_3 nanocrystals.[25,35-37]

Typically, the presence of the peak at 138 cm^{-1} stems from the

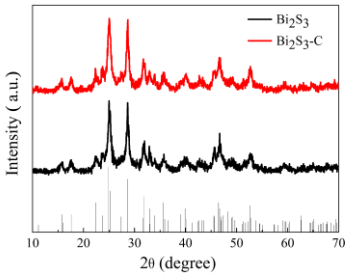

Fig.1 XRD patterns of as-synthesized Bi_2S_3 and Bi_2S_3-C.

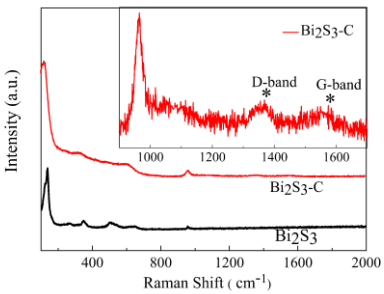

Fig. 2 Raman spectra of Bi_2S_3 and Bi_2S_3-C. The inset shows an enlarged profile of Bi_2S_3-C.

contribution of surface optical phonon modes.[38] From the partial enlarged drawing of Bi_2S_3-C Raman spectra (Inset of Fig.2), it can be found that two weak peaks appeared at 1355 and 1574 cm^{-1}. These two new peaks are corresponding to so-called D and G bands of carbon, respectively.[26,39] Energy dispersive spectroscopy (EDS) shown in Fig. S1 confirms the presence of C, S and Bi elements in Bi_2S_3-C microspheres.

The morphologies of the solvothermal synthesized Bi_2S_3 and Bi_2S_3-C samples were investigated by SEM, as shown in Fig. 3 and Fig. S2. The bare Bi_2S_3 (Fig. 3a) is composed of tremendous nanoparticles. In comparison, the facile synthesized Bi_2S_3-C composite product, as shown in Fig. 3b and Fig. 3c, exhibits the form of homogeneous porous microspheres with diameters of 2-3um. Furthermore, owing to the distribution of innumerable nanoparticles within the Bi_2S_3-C microspheres (Fig. 3d), this composite structure possesses a very large specific surface area.

In order to determine the microstructure of Bi_2S_3-C composite, TEM measurement was performed as shown in Fig.4. Fig. 4(a) shows that the diameter of Bi_2S_3-C microspheres is about 2.5 μm. From Fig. 4(b), it can be clearly seen that the synthesized Bi_2S_3-C microsphere possesses a highly porous structure. The high resolution TEM (HRTEM, Fig.4(c) and (d)) images reveal that the Bi_2S_3-C composite has good crystallinity and the lattice spacing of about 0.309 nm, which corresponds to the (211) facet. Besides, on the Bi_2S_3 particle surface there is an inhomogeneous coating layer, which is probably amorphous carbon derived from degradation of glucose.[26,40]

The porous character of the Bi_2S_3 and Bi_2S_3-C was analyzed by N_2 absorption and desorption measurements. As shown in Fig. 5, both of them exhibit a typical absorption-desorption isotherm of

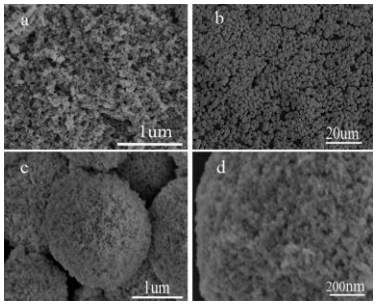

Fig.3 SEM images of as-prepared Bi_2S_3 (a) and Bi_2S_3-C (b-d).

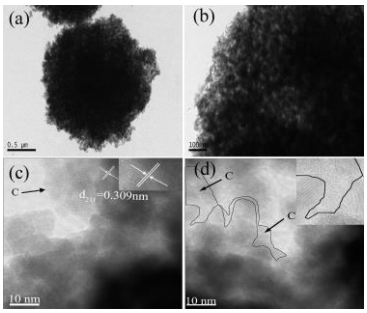

Fig. 4 (a) and (b)TEM images of Bi_2S_3-C. (c) and (d) HRTEM images of Bi_2S_3-C.

type IV. The Bi_2S_3-C composite possesses an ultrahigh BET surface area of 76.88 $m^2 \cdot g^{-1}$, which is close to that of Bi_2S_3 (77.31 $m^2 \cdot g^{-1}$). In addition, from the pore size distribution curves (inset of Fig. 5), they both have broad pore size distribution, from several nanometres to about 100 nm. The average pore diameter of the Bi_2S_3 is 14.6 nm with a pore volume of 0.282 $cm^3 \cdot g^{-1}$, while the average pore diameter of the Bi_2S_3-C microspheres increases to 14.9 nm with a pore volume of 0.286 $cm^3 \cdot g^{-1}$. The high surface area and rich mesopores structure of Bi_2S_3 and Bi_2S_3-C indicate that they are desirable for electrode materials because they can provide efficient electronic transportation channels during the oxidation-reduction process.

Photovoltaic performance of DSSCs

Fig. 6 and Fig. S3 present the photocurrent density-voltage (*J-V*) curves of DSSCs based on various CEs under the stand illumination (100 $mW \cdot cm^{-2}$). The corresponding photovoltaic parameters, such as the open-circuit voltage (V_{oc}), short-circuit current density (J_{sc}) and fill factor (*FF*), are summarized in Table 1. The conversion efficiency (η) of the DSSCs were calculated

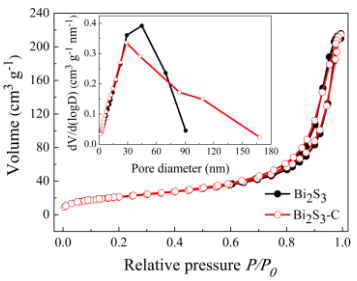

Fig. 5 N_2 absorption-desorption isotherms of the Bi_2S_3 and Bi_2S_3-C. Inset shows the corresponding BJH pore size distribution curves.

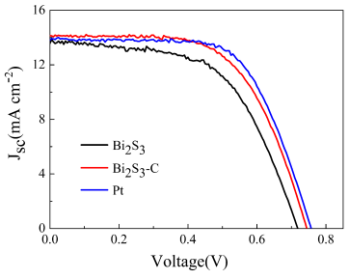

Fig. 6 Photovoltaic characteristics of the DSSCs using various CEs.

according to Eq. (1) and (2):

$$\eta(\%) = \frac{V_{oc} \times J_{sc} \times FF}{P_{in}} \times 100\% \quad (1)$$

and

$$FF = \frac{V_{max} \times J_{max}}{V_{oc} \times J_{sc}} \quad (2)$$

As shown in Table 1, the DSSC with the bare Bi_2S_3 CE exhibits an inferior photovoltaic conversion efficiency of 5.56% due to its poor electrocatalytic activity. However, after the optimization, the DSSC fabricated with Bi_2S_3-C microspheres CE presents a V_{oc} of 0.750 V, J_{sc} of 14.45 mA·cm^{-2}, and *FF* of 0.62, resulting in a promising conversion efficiency of 6.72%, which is very close to that of DSSC with traditional Pt CE (6.75%). Considering the detailed parameter of *FF*, we found that the addition of glucose in the preparation process of CEs leads to large differences in *FF* of DSSCs. As CEs for the DSSC, the Bi_2S_3-C exhibits much higher *FF* than the pure Bi_2S_3, which indicates the superiority of the former. The enhanced *FF* value may result from the positive synergistic effect between the Bi_2S_3 and amorphous carbon in the Bi_2S_3-C CEs. Therefore, the cooperation of Bi_2S_3 and amorphous carbon can effectively improve the catalytic performance of Bi_2S_3.

Electrochemical properties of CEs

In the following, the cyclic voltammetry (CV) tests, electrochemical impedance spectra (EIS) measurements, and Tafel polarization curves were used to investigate the electrocatalytic activities of various CEs.

Firstly, CV tests were carried out in a three-electrode system with the Pt sheet as CE, various CEs as working electrode and saturated calomel electrode as reference electrode. Fig. 7 and Fig. S4 show the CVs of various CEs in redox couple I^-/I_3^- system. Two typical pairs of oxidation and reduction peaks are observed for all CEs. The left pair in low potential range is assigned to the redox reaction Eq. (3) and the right pair in the high potential range is corresponded to the redox reaction Eq. (4):

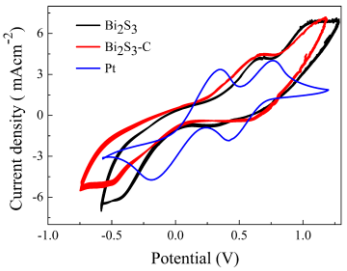

Fig. 7 CV curves for Bi_2S_3, Bi_2S_3-C and Pt electrodes

$$I_3^- + 2e^- \leftrightarrow 3I^- \quad (3)$$

$$3I_2 + 2e^- \leftrightarrow 2I_3^- \quad (4)$$

As can be seen in Fig. 7, the Bi_2S_3 and Bi_2S_3-C electrodes exhibit obvious cathodic peaks similar to that of the efficient Pt electrode, suggesting that the Bi_2S_3 and Bi_2S_3-C electrodes have similar catalytic ability to the Pt electrode. In addition, the reduction current peaks of Bi_2S_3-C electrode are higher than that of pure Bi_2S_3 electrode, which match well with the results of *J-V* curves and further confirm the higher catalytic activity of the former.

To further investigate the catalytic activities for regeneration of the redox couple I^-/I_3^- on the aforementioned CEs, EIS measurements were conducted in symmetrical cells fabricated with two identical CEs (CE/electrolyte/CE). As shown in Fig. 8 and Fig. S5, two typical semicircles are observed in the higher and lower frequency regions. The high-frequency intercept on the Z' axis is generally assigned to the Ohmic series resistance (R_s). The left semicircle is attributed to the charge-transfer resistance (R_{ct}) and the constant phase element (*CPE*) at the CE/electrolyte interface, while the right semicircle is consistent with the Nernst diffusion impedance (Z_W) in the electrolyte.[41] The corresponding EIS parameters are listed in Table 1. The Bi_2S_3 electrode possesses a large R_{ct} of 8.78 Ω·cm^{-2}. But after the addition of the carbon, the Bi_2S_3-C composite CEs demonstrate the lower R_{ct}. It's interesting that the R_{ct} of the Bi_2S_3-C CEs decreases gradually with increasing the dosage of carbon from 0.39 wt.% to 1.53 wt.%, and then increases with further increasing the carbon content. The change tendency of R_{ct} in the Bi_2S_3-C electrodes with different carbon contents is in agreement with that of other carbon-based materials, such as MoS_2/C,[18] MoS_2/G, [42] CoS_2/G[43] and WS_2/MWCNT.[44] This phenomenon maybe due to the excessive amounts of carbon reduces the catalytic activity of the Bi_2S_3-C. Ultimately, the sample of Bi_2S_3-1.53-C exhibits the smallest R_{ct} (2.26Ω·cm^{-2}) among all composite electrodes. This indicates that less resistance is required for the transfer of electrons from the surface of Bi_2S_3-1.53-C electrode to the electrolyte. In addition, the Bi_2S_3-C electrodes has smaller Z_W than that of the pristine Bi_2S_3 electrode, which indicates that the Bi_2S_3-C composite can provide more efficient electrolyte diffusion channel for I^-. Therefore, Bi_2S_3-C composite materials exhibit much higher catalytic activity than pure Bi_2S_3 material used as the CE for the DSSC, which is in agreement with the

results from above *J-V* and CV experiments.

Table 1 Photovaltaic and EIS parameters of the different CEs

CEs	V_{oc} (V)	J_{sc} (mA·cm^{-2})	*FF*	η (%)	R_s (Ω·cm^{-2})	R_{ct} (Ω·cm^{-2})	Z_W (Ω·cm^{-2})
Bi_2S_3	0.718	13.68	0.57	5.56	6.30	8.78	1.04
Bi_2S_3-0.39-C	0.729	14.03	0.58	5.89	7.31	5.42	1.03
Bi_2S_3-0.77-C	0.744	14.14	0.60	6.36	7.18	3.65	0.80
Bi_2S_3-1.53-C	0.750	14.45	0.62	6.72	7.22	2.26	0.39
Bi_2S_3-2.28-C	0.725	13.92	0.58	5.88	7.43	6.74	0.80
Pt	0.757	13.82	0.64	6.75	4.10	1.67	0.30

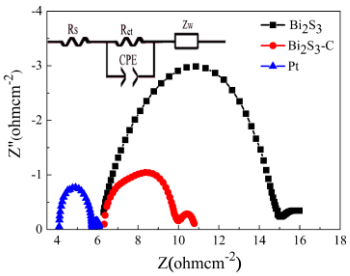

Fig. 8 Electrochemical impedance spectra of different CEs. Inset figure is the equivalent circuit model.

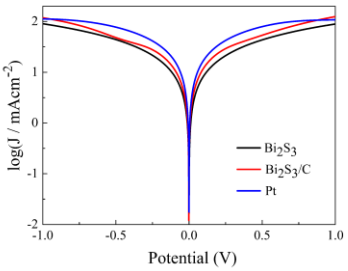

Fig.9 Tafel curves of the symmetric cells based on various electrodes.

Finally, Tafel polarization analysis was executed using symmetric cells similar to the one used in above EIS experiments. Fig.9 shows the Tafel polarization curves for the Bi_2S_3, Bi_2S_3-C and Pt electrodes. In general, exchange current density (J_0) and limiting diffusion current density (J_{lim}) are closely related to the catalytic activity of the catalysts.[45] In Fig. 9, the Bi_2S_3-C composite electrode shows a larger slope in the anodic and cathodic branches than the Bi_2S_3 electrode, suggesting a higher J_0 in the Bi_2S_3-C electrode surface. Obviously, the slope of Pt electrode is the highest one, implying that the highest J_0 and best catalytic activity of Pt electrode among these CEs. Furthermore, J_0 can also be estimated by Eq. (5):

$$J_0 = RT/(nFR_{ct}) \quad (5)$$

where *R* is the gas constant, *T* is the absolute temperature, *F* is Faraday's constant and *n* represents the number of electrons involved in the reduction of I_3^- at the electrode. The tendency of J_0 for three CEs calculated according to above equation coincide well with that obtained from the Tafel polarization curves. In addition, the Tafel curves also include the information of J_{lim}, which can be expressed by Eq. (6):

$$J_{min} = 2nFCD/l \quad (6)$$

where *C* is the I^-/I_3^- concentration, *D* is the diffusion coefficient of the I_3^- in electrolyte and *l* is the spacer thickness. From Eq. (6), a higher J_{lim} indicates a lager diffusion coefficient *D* of the I_3^- in electrolyte at same potential. Meanwhile, a CE with a faster diffusion rate of the I_3^- represents its smaller Nernst diffusion impedance Z_W in the electrolyte. Apparently, the order of J_{lim} is Pt > Bi_2S_3-C > Bi_2S_3 in Fig. 9, which is completely consistent with the order of Z_W in EIS spectra. This result suggests that Bi_2S_3-C nanocomposites possess a higher catalytic activity for the reduction of I_3^- than Bi_2S_3.

Fig. 10 shows the possible synergistic effect on the improved electrocatalytic ability of the Bi_2S_3-C composite. The grain boundary in the CEs assembled by Bi_2S_3 nanoparticles may cause the poorly efficient migration of electrons, due to the electron scattering in this crystal boundary.[46] In the Bi_2S_3-C composites, this electron scattering may be overcome by the conductive carbon that covers the Bi_2S_3 particles. In addition, when the electrons flow into the CEs, they are easily shuttled to the intrinsically electrocatalytic Bi_2S_3 by taking advantage of the fast electron transport network of carbon. As a result, the excellent conductivity of the amorphous carbon and the superior electrocatalytic activity of the Bi_2S_3 can provide low R_{ct} at the interface between the CE and electrolyte for the I^-/I_3^- redox reaction. Notably, the excessive amounts of carbon could reduce the catalytic activity of the Bi_2S_3-C. With the excessive increase of the carbon contents, the amorphous carbon heavily surrounds Bi_2S_3 nanoparticles in a microsphere of Bi_2S_3-C composite, leading to the isolation of Bi_2S_3 from redox couple I^-/I_3^- system, reducing the catalytic activity of the Bi_2S_3 and R_{ct} enhanced. The two effects compete with other. Consequently, the Bi_2S_3-1.53-C CE has the fastest electron-transfer kinetics than other CEs due to the synergistic effect from the conductive network of carbon and the intrinsically catalytic Bi_2S_3, and the DSSCs with it obtain the highest conversion efficiency.

Conclusion

In this study, a nanocomposites of Bi_2S_3-C was successfully prepared by a facial one-step solvothermal method. The compositions and morphologies of Bi_2S_3-C composite material were observed by XRD, Raman, SEM, TEM and EDS. In addition, *J-V* curves, CV, EIS and Tafel polarization experiments have demonstrated the superiority of the composite electrode, which is mainly due to the positive synergistic effect in the

combined Bi_2S_3-C composite, including improved electrical conductivity and enhanced electrocatalytic activity for I_3^- reduction. As a result, the DSSCs fabricated with the Bi_2S_3-C CE obtained a high conversion efficiency of 6.72 % by the optimization of the carbon content in composite materials, which increased by more than 20% compared with that of bare Bi_2S_3 CE, suggesting Bi_2S_3-C composite materials is a potential alternative to expensive Pt for the low-cost DSSCs.

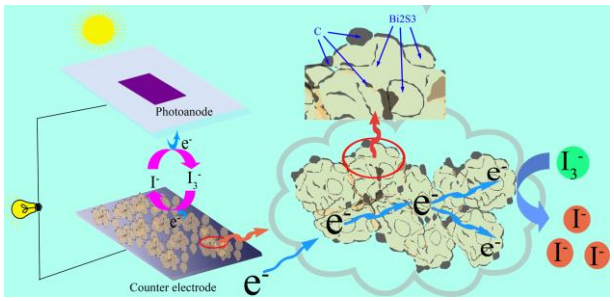

Fig.10 Schematic for the possible synergistic effect on the improved electrocatalytic ability of the Bi_2S_3-C composite.

Acknowledgements

This work was financially supported by the State Key Program for Basic Research of China (No. 2013CB632705), National Natural Science Foundation of China (11174002), '211 Project' of Anhui University and by Anhui Provincial Education Department for Scientific Research of College and Universities (KJ2013A018).

References

1 B. O'Regan and M. Grätzel, *Nature*, 1991, **353**, 737.
2 M. Grätzel, *Nature*, 2001, **414**, 338.
3 W. Q. Fang, X. H. Yang, H. J. Zhu, Z. Li, H. J. Zhao, X. D. Yao and H. G. Yang, *J. Mater. Chem.*, 2012, **22**, 22082
4 X. Yin, B. Wang, M. He and T. He, *Nano Res.*, 2012, **5**, 1.
5 J. X. Shi, Y. X. Liu, Q. Peng and Y. D. Li, *Nano Res.*,2013, 6, 441.
6 J. T. Zhang, M. He, N. Q. Fu, J. Y. Li and X. Yin, *Nanoscale*, 2014, 6, 4211.
7 J. K. Chen, K. X. Li, Y. H. Luo, X. Z. Guo, D. M. Li, M. H. Deng, S. Q. Huang and Q. B. Meng, *Carbon*, 2009, **47**, 2704.
8 T. Peng, W. W. Sun, X. H. Sun, N. Huang, Y. M. Liu, C. H. Bu, S. S. Guo and X. Z. Zhao, *Nanoscale*, 2013, **5**, 337.
9 K. H. Yu, Z. H. Wen, H. H. Pu, G. H. Lu, Z. Bo, H. Kim, Y. Y. Qian, E. Andrew, S. Mao and J. H. Chen, *J. Mater. Chem. A*, 2013, **1**, 188.
10 T. H. Lee, K. Do, Y. W. Lee, S. S. Jeon, C. Kim, J. Kob and S. S. Im, *J. Mater. Chem.*, 2012, **22**, 21624.
11 S. J. Peng, P. N. Zhu, Y. Z. Wu, S. G. Mhaisalkar and S. Ramakrishna, *RSC Advances*, 2012, **2**, 652.
12 Q. W. Tang, H. Y. Cai, S. S. Yuan and X. Wang, J. *Mater.Chem. A*, 2013, **1**, 317.
13 M. Al-Mamun, H. M. Zhang, P. R. Liu, Y. Wang, J. Cao and H. J. Zhao, *RSC Advances*, 2014, **4**, 21277.
14 J. Song, G. R. Li, F. Y. Xiong and X. P. Gao, *J. Mater.Chem.*, 2012, **22**, 20580.
15 M. X. Wu, X. Lin, A. Hagfeldt and T. L. Ma, *Chem. Commun.*, 2011, **47**, 4535.
16 M. K. Wang, A. M. Anghel, B. Marsan, N. L. C. Ha, N. Pootrakulchote, S. M. Zakeeruddin and M. Grätzel, *J. Am. Chem. Soc.*, 2009, **131**, 15976.
17 W. Zhao, T. Q. Lin, S. R. Sun, H. Bi, P. Chen, D. Y. Wan and F. Q. Huang, *J. Mater. Chem. A*, 2013, **1,** 194.
18 G. T. Yue, J. H. Wu, Y. M. Xiao, M. L. Huang, J. M. Lin and J. Y. Lin, *J. Mater. Chem. A*, 2013, **1**, 1495.
19 X. Yang, L. Zhou, A. L. Feng, H. B. Tang, H. J. Zhang, Z. L. Ding, Y. Q. Ma, M. Z. Wu, S. W. Jin and G. Li, *J. Materials Research*, 2014, **29**, 935.
20 B. Yang, X. Q. Zuo, H. J. Xiao, L. Zhou, X. Yang, G. Li, M. Z. Wu,Y. Q. Ma, S. W. Jin and X. S. Chen, *Mater Lett*, 2014, **133**, 197
21 H. J. Zhang, M. Ge, L. T. Yan, Z. Zhou, W. Chen, Q. Z. Li and L. Liu, *J. Phys. Chem. C*, 2013, **117**, 10285.
22 R. Suarez, P. K. Nair and P. V. Kamat, *Langmuir*, 1998, **14**, 3236.
23 L. Li, N. Sun, Y. Huang, Y. Qin, N. Zhao, J. Gao, M. Li, H. Zhou and L. Qi, *Adv. Funct. Mater.*, 2008, **18**, 1194.
24 B. Zhang, X. C. Ye, W. Y. Hou, Y. Zhao and Y. Xie, *J. Phys. Chem. B*, 2006, **110**, 8978.
25 Z. A. Zhang, C. k. Zhou, H. Lu, M. Jia, Y. Q. Lai and J. Li, *Mater Lett*, 2013, **91**, 100.
26 Y. Zhao, D. L. Gao, J. F. Ni, L. J. Gao, J. Yang and Y. Li, *Nano Res.*, 2014, **7**, 765.
27 L. M. Peter, K. G. U. Wijayantha, D. J. Riley and J. P. Waggett, *J. Phys. Chem. B*, 2003, **107**, 8378.
28 H. J. Zhang, L. T. Yang, Z. Liu, M. Ge, Z. Zhou, W. Chen, Q. Z. Li and L. Liu, *J. Mater. Chem.*, 2012, **22**, 18572.
29 J. F. Wang, Z. Liu, S. M. Yuan, L. Liu, Z. Zhou and W. Chen, *Aust. J. Chem.*, 2012, **65**, 1342.
30 G. Li, X. S. Chen and G. D. Gao, *Nanoscale*, 2014, **6**, 3283.
31 M. X. Wu, X. Lin, A. Hagfeldt and T. L. Ma, *Angew. Chem., Int. Ed.*, 2011, **50**, 3520.
32 G. R. Li, F. Wang, J. Song, F. Y. Xiong and X. P. Gao, *Electrochim. Acta*, 2012, **65**, 216.
33 Y. Y. Wang, S. J. Li, Y. Bai, Z. Chen, Q. W. Jiang, T. Li and W. F. Zhang, *Electrochim. Acta*, 2013, **114**, 30.
34 J. F. Ni, M. Morishita, Y. Kawabe, M. Watada, N. Takeichi and T. Sakai, *J. Power Sources*, 2010, **195**, 2877.
35 O. Rabin, J. M. Perez, J. Grimm, G. Wojtkiewicz and R. Weissleder, *Nat. Mater.*, 2006, **5**, 118.
36 Y. W. Koh, C. S. Lai, A. Y. Du, E. R. T. Tiekink and K. P. Loh, *Chem. Mater.*, 2003, **15**, 4544.
37 Y. J. Xiao, H. Q. Cao, K. Y. Liu, S. C. Zhang and V. Chernow, *Nanotechnology*, 2010, **21**, 145601.
38 X. H. Yang, X. Wang and Z. D. Zhang, *Mater. Chem. Phys.*, 2006, **95** 154.
39 A. C. Ferrari, *Solid State Communications*, 2007, **143**, 47.
40 J. Liu, J. Ni, Y. Zhao, H.Wang and L. Gao, *J. Mater. Chem. A*, 2013, **1**, 12879.
41 G. Li, F. Wang, Q. Jiang, X. Gao and P. Shen, *Angew. Chem., Int. Ed.*, 2010, **49**, 3653.
42 J. Y. Lin, G. T. Yue, S. Y. Tai, Y. M. Xiao, H. M.Cheng, F. M. Wang and J. H. Wu, *Mater. Chem. Phys.*, 2013, **143**, 53.
43 X. L. Duan, Z. Y. Gao, J. L. Chang, D. P. Wu, P. F. Ma, J. J. He, F. Xu, S. Y. Gao and K. Jiang, *Electrochim. Acta*, 2013, **114**, 173.
44 G. T. Yue, J. H. Wu, J. Y. Lin, Y. M. Xiao, S. Y. Tai, J. M. Lin , M. L. Huang and Z. Lan, *Carbon* , 2013, **55**, 1.
45 C. J. Liu, S. Y. Tai, S. W. Chou, Y. C. Yu, K. D. Chang, S. Wang, F. S. S. Chien, J. Y. Lin and T. W. Lin, *J. Mater. Chem.*, 2012, **22**, 21057.
46 Y. P. Liao, K. Pan, L. Wang, Q. J. Pan, W. Zhou, X. H. Miao, B. J. Jiang, C. G. Tian, G. H. Tian, G. F. Wang and H. G. Fu, *ACS Appl. Mater. Interfaces*, 2013, **5**, 3663.